FEBS Letters 580 (2006) 4143–4149

The non-structural protein Nsp10 of mouse hepatitis virus binds zinc ions and nucleic acids

Nele Matthes[a], Jeroen R. Mesters[a], Bruno Coutard[b], Bruno Canard[b], Eric J. Snijder[c], Ralf Moll[a], Rolf Hilgenfeld[a,*]

[a] *Institute of Biochemistry, Center for Structural and Cell Biology in Medicine, University of Lübeck, 23538 Lubeck, Germany*
[b] *AFMB UMR6098 CNRS/Université Aix-Marseille I & II, Case 932, 163 Avenue de Luminy, 13288 Marseille Cedex 09, France*
[c] *Molecular Virology Laboratory, Department of Medical Microbiology, Center of Infectious Diseases, Leiden University Medical Center, P.O. Box 9600, 2300 RC Leiden, The Netherlands*

Received 19 April 2006; revised 6 June 2006; accepted 15 June 2006

Available online 30 June 2006

Edited by Lev Kisselev

Abstract The non-structural protein Nsp10 of coronaviruses is a small cleavage product of the viral replicase polyprotein that has been implicated in RNA synthesis. Nsp10 of mouse hepatitis virus (MHV) displays an apparent molecular mass of 13–16 kDa in reducing SDS–PAGE and analytical gel filtration, while dynamic light scattering suggests the existence of oligomeric forms. Atomic absorption spectroscopy reveals two metal ions per Nsp10 monomer, with a preference for Zn^{2+} over $Fe^{2+/3+}$ and Co^{2+}. These are probably bound by two Zn-finger-like motifs. Moreover, MHV Nsp10 interacts with tRNA, single-stranded RNA, double-stranded DNA and, to a lesser extent, single-stranded DNA as shown by gel-shift experiments. The K_d for tRNA is 2.1 ± 0.2 μM.

Keywords: Non-structural protein; Nsp10; Mouse hepatitis virus; Zinc finger; RNA/DNA binding protein; Zone-interference gel electrophoresis

1. Introduction

Murine hepatitis virus (MHV) is a positive-strand RNA virus of the family *Coronaviridae* that possess genomes of approx. 31 300 nucleotides. MHV has been taxonomically assigned to coronavirus group 2 and is thus a phylogenic neighbour of SARS coronavirus [1], the etiological agent of severe acute respiratory syndrome (see, e.g., [2] for review). Depending on the strain, MHV can cause hepatitis, encephalitis and demyelinating encephalomyelitis in susceptible rodents [3] and the virus has been used as a model system for infection of the central nervous system (CNS) [4] and virus-induced autoimmune reactions in the CNS [5]. Coronavirus genomes contain up to 15 open reading frames encoding both structural and non-structural proteins [6,7]. From the largest open reading frames, 1a and 1b, two polyproteins are translated, pp1a (~500 kDa) and pp1ab (~800 kDa), the latter originating from a (−1)-ribosomal frameshift occurring in the short overlap region of orf 1a and orf 1b. The two MHV polyproteins are cleaved into 16 non-structural proteins [8] by two papain-like proteinases, $PL1^{pro}$ and $PL2^{pro}$, which are part of Nsp3 [9], and by the main proteinase (M^{pro}, Nsp5), which is frequently also called 3C-like proteinase ($3CL^{pro}$) [10,11]. Most or all of the 16 non-structural proteins are proposed to be part of the replicase–transcriptase complex, probably mediating all functions necessary for polyprotein processing, viral transcription, and replication [6]. After translation and processing, MHV non-structural proteins form replication complexes that are thought to be associated with multilayered membrane structures [12] or double-membrane vesicles [13]. Most MHV replicase subunits were found to co-localize in discrete foci in the perinuclear region of the infected cell [12–15]. Dual-labelling studies demonstrated co-localization of, e.g. Nsp8 with the helicase (Nsp13), the nucleocapsid protein, the main proteinase (Nsp5), Nsp7, 9, and 10 [15]. Moreover, Nsp1 specifically binds to Nsp7 and Nsp10 as shown by yeast-two-hybrid and co-immunoprecipitation experiments [16]. These examples of interactions between coronavirus Nsps are likely to be the tip of an iceberg of protein–protein interactions that drive the formation of the replication–transcription complex and, probably, are critical to its function. In temperature-sensitive mutants of MHV-A59 [7], mutations assigned to Nsp4, 5, 10, 12, 14, and 16 are responsible for a variety of defects in RNA synthesis. Therefore, these proteins are assumed to be essential components of the replicase–transcriptase and to fulfil distinct functions in negative- and/or positive-strand RNA synthesis.

In this communication, we describe the biochemical characterization of MHV Nsp10. The avian infectious bronchitis virus (IBV) Nsp10 homolog was reported to be membrane-associated in one report [17], while another [18] predicted "growth-factor-like" properties on the basis of the presence of a cysteine-rich motif near the C-terminus of the protein. Although the cysteines were substituted by alanines in mutagenesis experiments [17], the residues involved in dimerization could not be assigned unambiguously. Interestingly, a temperature-sensitive MHV Nsp10 mutant, in which the highly conserved Gln65 was substituted by Glu, appeared to be defective in continuing negative-strand RNA synthesis [7].

*Corresponding author. Fax: +49 451 500 4068.
E-mail address: hilgenfeld@biochem.uni-luebeck.de (R. Hilgenfeld).

Abbreviations: CNS, central nervous system; IPTG, isopropyl-β-thiogalactoside; Ni-NTA, nickel nitrilotriacetic acid; SDS–PAGE, sodium dodecyl sulfate–polyacrylamide gel electrophoresis; TY, tryptone-yeast

0014-5793/$32.00
doi:10.1016/j.febslet.2006.06.061

Here we show MHV Nsp10 to bind zinc ions with preference over ferric/ferrous iron and cobalt ions. Based on these results, two C-terminal cysteine-rich motifs are proposed to constitute zinc fingers coordinating the metal ions. Moreover, Nsp10 is shown to bind nucleic acids as demonstrated by native agarose and zone-interference gel electrophoresis (ZIGE).

2. Materials and methods

2.1. Virus, plasmid and cells

The genome of a recombinant vaccinia virus (vMHV-inf-1) carrying a full-length cDNA copy of the MHV-A59 genome [19] was used as template to PCR-amplify the Nsp10-coding sequence using the following primers: GGGGACAAGTTTGTACAAAAAAGCAGGCTTCGAAGGAGATGCCACCATGAAACATCACCATCACCATCACgcgggtacggcaactgagtatgcc (forward) and GGGGACACTTTGTACAAGAAAGCTGGGTCTTATTActgaaactgggagcctgtgcctac (reverse). The forward primer also coded for an N-terminal His_6-tag without additional spacer residues between the tag and the authentic protein. The resulting PCR product was cloned via the Gateway® system into a pDEST14 expression vector (Invitrogen). After transformation of the plasmid into *Escherichia coli* C43 (DE3) cells (Avidis), expression was performed for 24 h at 25 °C. Cells were grown on 4× tryptone-yeast (TY) supplemented either with 0.5 mM $ZnCl_2$ (yielding Nsp10 + Zn), 1 mM $CoCl_2$ (Nsp10 + Co), 0.5 mM $FeSO_4$ (stabilized by ascorbate; Nsp10 + Fe), or no additional metal ions (Nsp10-Me) before induction with 0.5 mM isopropyl-β-thiogalactoside (IPTG).

2.2. Protein purification

The cells were resuspended in lysis buffer (50 mM Tris–HCl, 300 mM NaCl, 25 mM imidazole, 0.25 mg/ml lysozyme, pH 8.0) and disrupted by French Press. After ultracentrifugation at $160000 \times g$ (60 min, 4 °C), the supernatant was applied onto a nickel nitrilotriacetic acid (Ni-NTA) affinity column (GE HealthCare). Nsp10 was eluted using a gradient from 10 to 500 mM imidazole. Fractions containing Nsp10 were pooled and concentrated with an Amicon ultrafiltration stirring cell using a YM membrane (3 kDa cut-off; Millipore). The protein was further purified by gel filtration (Superdex 200 16/60, GE HealthCare) in 10 mM Tris–HCl, 100 mM NaCl, pH 7.5. All protein samples used in the experiments described below contained this buffer. Before storage at 4 °C, 20 mM glutathione was added to protein fractions that had been produced without additional metal ions, in order to increase Nsp10 solubility. Protein fractions were subjected to sodium dodecyl sulfate–polyacrylamide gel electrophoresis (SDS–PAGE) and Western blotting. Blots were probed with anti-tetrahistidine antibodies (Dianova) and anti-mouse IgG-alkaline phosphatase conjugate (Sigma). Nitro tetrazolium salt and 5-bromo-4-chloro-3-indolylphosphate were added as substrates for colour detection. The protein concentration was determined by the method outlined in [20].

2.3. Analytical size-exclusion chromatography

The apparent molecular mass of the Nsp10 protein derived from Zn-supplemented cultures (Nsp10 + Zn) was determined by an analytical BioSep-SEC-S 3000 column (Phenomenex) connected to an HPLC DuoFlow (BioRad). The column was calibrated in 20 mM Tris–HCl, 200 mM NaCl, pH 7.0, using the following standard proteins: cytochrome *c* (12.5 kDa), chymotrypsinogen (25.0 kDa), ovalbumin (42.75 kDa), bovine serum albumin (66.41 kDa), glucose oxidase (160 kDa), and thyroglobulin (670 kDa). The Nsp10 + Zn solution had a concentration of 10 mg/ml. The sample volume was 25 µl.

2.4. Dynamic light scattering

Dynamic light scattering (DLS) was performed using a Laser-Spectroscatter 201 (RiNA GmbH). Before measurement, samples were centrifuged for 1 h at 4 °C and $17900 \times g$. 20 µl-samples were applied to quartz cuvettes with a light path of 10 and 1.5 mm-width of the light-accessible window (Hellma). In experiments with samples containing oligonucleotides, the latter were added as a nearly equimolar aqueous solution (see Fig. 4 for details).

2.5. Atom-absorption spectroscopy

Amounts of the elements zinc, cobalt and iron were measured in purified Nsp10 samples using a polarized Zeeman Atom Absorption Spectrometer 180-80 with an uncoated tube cuvette (Hitachi). A dilution series was used for standard measurements with stock solutions of $Zn(NO_3)_2$, $Fe(NO_3)_3$, and $Co(NO_3)_2$. The concentrations of the standard solutions ranged from 0 to 1 µM for zinc and from 0 to 10 µM for cobalt and iron.

2.6. Native agarose gel electrophoresis and zone-interference gel electrophoresis

Native gels were run in 20 mM MES, 50 mM NaCl, 3.5 mM $MgCl_2$, pH 6.0, in horizontal 1% (w/v) agarose gels with 50 V/200 mA for 2 h at 4 °C. The protein concentration in the samples was 10 µM. Nsp10 samples were incubated for 10 min at room temperature with 10 µM tRNA, 10 µM single-stranded DNA (28 mer), 50 µM double-stranded DNA (28 mer), or 20 µM single-stranded RNA (20 mer). The ZIGE device was adapted from [21]. The sample application comb for protein

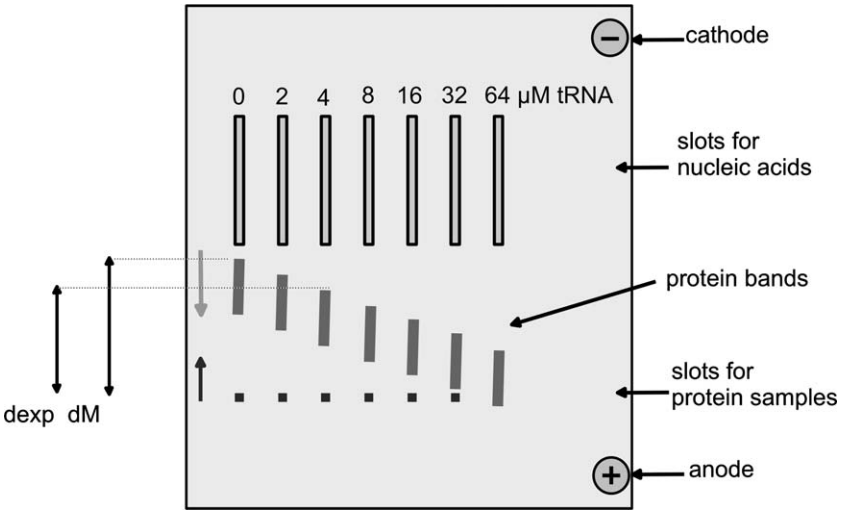

Fig. 1. Schematic view of the modified ZIGE. Black and grey arrows indicate the direction of protein and nucleic acid migration in the agarose gel system, respectively. Increasing concentrations of nucleic acid are added to the upper slots, whereas a constant concentration of protein is applied to the lower slots. d_{exp}, experimentally observed migration distance of the protein in the presence of nucleic acids; d_M, migration distance of the protein in the absence of ligand.

and nucleic acids had to be modified according to Fig. 1, because Nsp10 and nucleic acids migrate in opposite directions at pH 6.0. The agarose was dissolved in running buffer (20 mM MES, 50 mM NaCl, 3.5 mM $MgCl_2$, pH 6.0). Electrophoresis was performed at 4 °C. The protein samples were mixed with dimethylsulfoxide (DMSO) with a final concentration of 10% (v/v) and a trace of bromophenolblue (BPB) dye. 10 μl-sample volumes with protein concentrations of 40 μM were applied to the small slots. The electrophoresis was started with a constant current of 200 mA for 30 min. Afterwards, tRNA was mixed with DMSO and BPB as well and applied to the long slots of the gel. The final concentrations were 0, 2, 4, 8, 16, 32, and 64 μM deacetylated *E. coli* tRNA in a sample volume of 100 μl. The run was continued for 90 min under the same conditions as before. The staining procedure was performed as outlined in [21]. The gels were scanned to facilitate the measurement of the d_{exp}- and d_M-values (see Fig. 1 for definition) for the calculation of K_d-values. By plotting $(d_{exp} - d_M)/[tRNA]$ against d_{exp}, K_d can be derived according to

$$\frac{d_{exp} - d_M}{[tRNA]} = \frac{d_{exp} - d_{ML}}{K_d}.$$

The slope of the resulting linear function gives $-1/K_d$.

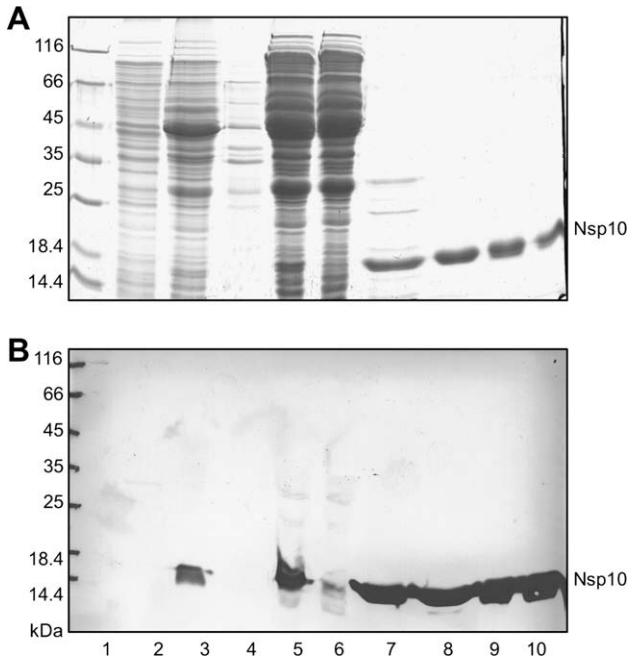

Fig. 2. Overproduction and purification of histidine-tagged MHV Nsp10. (A) SDS–PAGE, (B) Western blot. Lane 1, molecular weight marker; lane 2, *E. coli* lysate before induction with IPTG; lane 3, lysate after induction of the *nsp10* gene expression; lane 4, proteins from the pellet after ultracentrifugation; lane 5, proteins of the cytosolic supernatant; lane 6, proteins of the flow-through fraction of the Ni-NTA affinity chromatography; lane 7, Nsp10 after elution with imidazole in Ni-NTA chromatography; lanes 8–10, peak fractions of Nsp10 after preparative Superdex gel filtration.

3. Results

3.1. Expression and purification of MHV-A59 Nsp10

The yield of Nsp10 after expression in *E. coli* C43 (DE3) cells was about 25 mg/L culture. The presence of an N-terminal hexahistidine tag allowed efficient purification by Ni-NTA agarose affinity chromatography. After subsequent size-exclusion chromatography, a relatively pure protein preparation was obtained that exhibited an apparent molecular mass of ~16 kDa in denaturing and reducing SDS–PAGE (Fig. 2A). This value agreed well with the molecular mass deduced from the amino-acid sequence (15.4 kDa). Owing to the hexahistidine tag, the Nsp10 could be readily detected in immunoblots using an anti-tetrahistidine antibody (Fig. 2B). In the non-reducing SDS–PAGE, a faint band, possibly corresponding to a dimeric form, was detected in addition to the main band (not shown). Remarkably, Nsp10 preparations obtained from cultures that had been supplemented with either cobalt (Nsp10 + Co) or iron ions (Nsp10 + Fe), were coloured blue and light red, respectively, during gel filtration. The colour remained after ultrafiltration, while the flow-through was colourless. Apparently, the Nsp10 protein had bound these metal ions tightly.

3.2. Oligomerization state of Nsp10

Upon gel filtration, Nsp10 obtained from Zn-supplemented cultures (Nsp10 + Zn) eluted as a single peak corresponding to a molecular mass of 13.6 kDa, suggesting a monomeric state of the protein under these conditions (Fig. 3B). In contrast, dynamic light scattering of Nsp10 revealed several different states

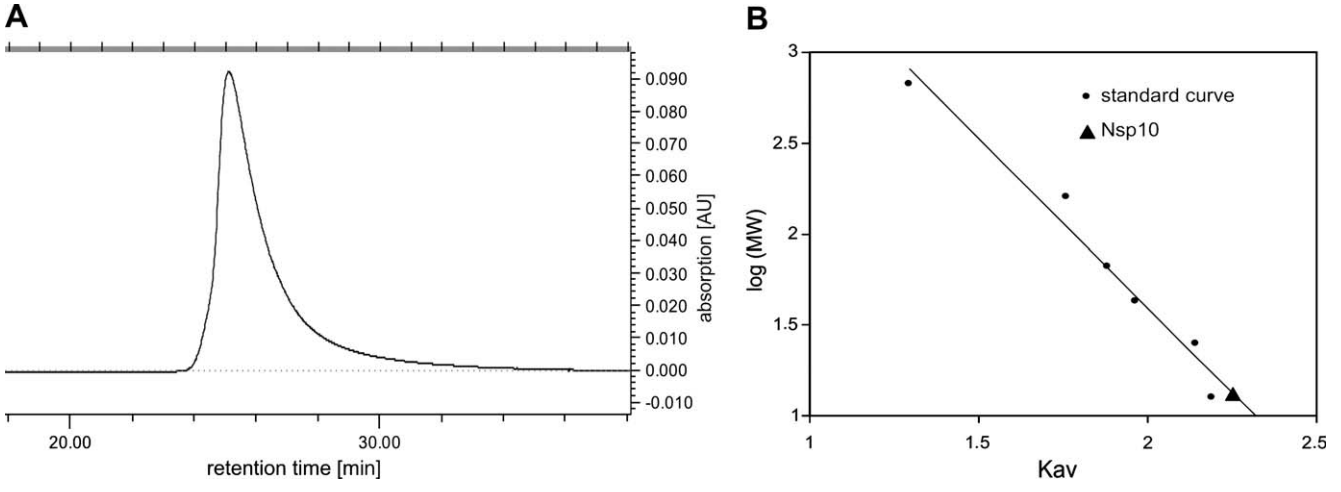

Fig. 3. Analytical gel filtration of the MHV Nsp10 protein. (A) Gel filtration chromatogram of Zn-supplemented Nsp10. (B) Calibration curve of the analytical column. Nsp10 is marked with a triangle. $K_{av} = (V_e - V_0/V_t - V_0)$; V_e, elution volume; V_0, void volume; V_t, total volume; MW, calculated molecular mass.

of oligomerization, depending on the conditions applied (Fig. 4). In the absence of metal ion supplements, but with 20 mM glutathione present, the protein solution (2.8 mg/ml) showed a monodisperse peak at a Stokes radius of 9 nm (Fig. 4A). Assuming the corresponding Nsp10 oligomer to be spherical, a molecular mass of around 600 kDa, corresponding to higher-order aggregates, can be calculated from this. Nsp10 + Zn, Nsp10 + Co, and Nsp10 + Fe samples tended to be polydisperse (Figs. 4B–D) and the intensity of the peaks decreased. The following main peaks were observed in these samples: Nsp10 + Zn at 3.9 and 38 nm (corresponding to an 80 kDa and to a very large aggregate, respectively); Nsp10 + Co at 6 nm (223 kDa), and Nsp10 + Fe at 2.4 nm (24.2 kDa). The cobalt-supplemented protein displayed the most polydisperse distribution among these DLS measurements. Interestingly, when double-stranded oligodeoxynucleotides were added to the Nsp10 + Zn solution, all indications of an oligomeric association state vanished and a clear, monodisperse signal at a Stokes radius of 2.0 nm, corresponding to a 16.3 kDa Nsp10 monomer, was observed (Fig. 4E). When a single-stranded oligodeoxynucleotide was added, a more polydisperse pattern with a main peak at a Stokes radius of 2.2 nm resulted (Fig. 4F).

3.3. Binding of metal ions

Amounts of metal ions bound to Nsp10 were measured using atomic absorption spectrometry. MHV Nsp10 was found to be a metalloprotein that favours zinc-ion binding over ferrous/ferric ion and Co^{2+} (Table 1). Nsp10 purified from expression cultures not supplemented with any metal ion (Nsp10-Me) bound 0.8 Zn^{2+} per Nsp10 monomer. The Zn^{2+} content of Nsp10 + Zn was up to 1.84 ions Zn^{2+} per Nsp10 monomer. Remarkably, Nsp10 + Co and Nsp10 + Fe preparations exhibited a 3–4 times higher content of Zn^{2+}

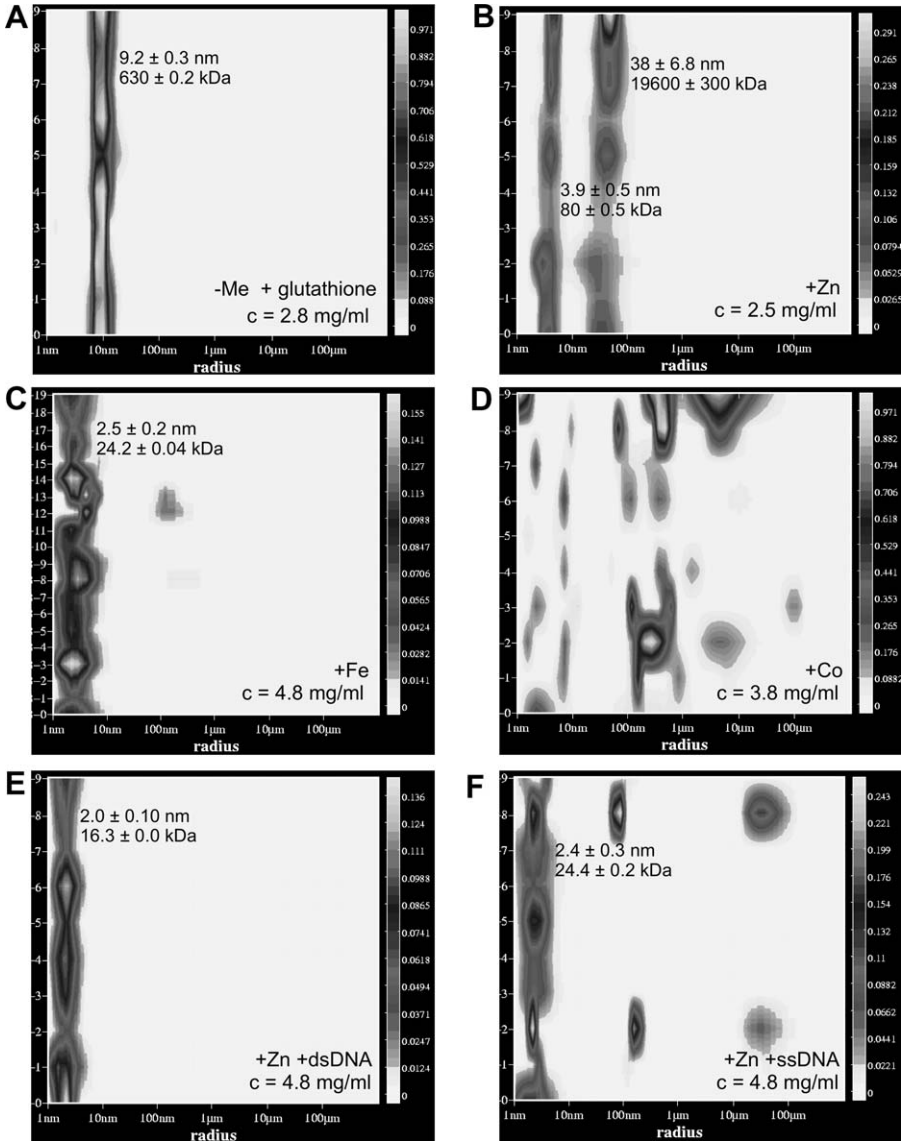

Fig. 4. Dynamic light scattering of differently treated MHV Nsp10 samples. The metal ion added during growth of the bacteria is indicated. In image (A), no metal salt was added to the culture, but 20 mM glutathione was added to the sample after purification. The abscissa shows the particle radius, the ordinate the number of measurements.

Table 1
Metal-ion content of heterologously produced MHV Nsp10 proteins

	Nsp10-Me	Nsp10 + Zn	Nsp10 + Co	Nsp10 + Fe
Zinc	0.8	1.84	1.45	1.07
Iron	No data	0.25	0.17	0.33
Cobalt	No data	0.06	0.34	0.02
$\sum$	No data	2.15	1.96	1.42

Number of metal ions bound per Nsp10 monomer. Nsp10 proteins were isolated from growing *E. coli* cultures supplemented either with zinc-, ferrous iron- or cobalt salts as described in Section 2. Where no additional metal salts were added to growing cultures, the isolated Nsp10 protein was stored in the presence of 20 mM reduced glutathione (column 'Nsp10-Me').

compared to Co^{2+} or $Fe^{2+/3+}$, even though the cells were grown in the presence of very high concentrations of the latter. Presumably, the zinc ions originated from the 4× TY medium that was used in growing the cells. The lowest total metal ion content was displayed by Nsp + Fe samples (Table 1). Nevertheless, also in the Zn^{2+}-supplemented sample (Nsp10 + Zn), about 12% of the total metal ion content was contributed by ferrous/ferric ions. In the Nsp10 + Zn and the Nsp10 + Fe samples, there was almost the same amount of iron bound, clearly indicating the preference of Nsp10 for Zn^{2+} over $Fe^{2+/3+}$. Only minor amounts of Co^{2+} were detected in Nsp10 + Zn and Nsp10 + Fe samples, suggesting that among the three metal ions tested, Co^{2+} has the lowest binding affinity to Nsp10.

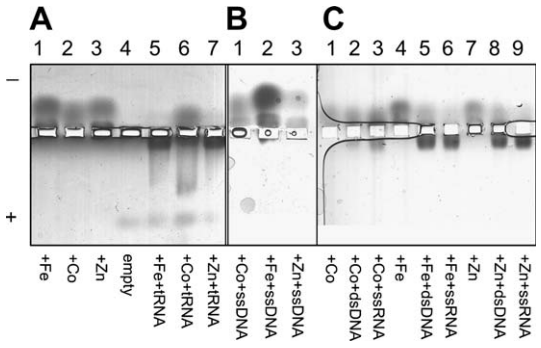

Fig. 5. Native agarose gel electrophoresis of Nsp10 incubated with different oligonucleotides. (A) Nsp10 without any oligonucleotides can be seen in lanes 1–3. Lanes 5–7 show Nsp10 in complex with tRNA. The lower band corresponds to free tRNA. (B) Nsp10 incubated with a single-stranded 28 mer oligodeoxynucleotide. (C) Nsp10 in complex with a double-stranded 28 mer oligodeoxynucleotide (lanes 2, 5, and 8); with a single-stranded 20 mer oligoribonucleotide (lanes 3, 6, and 9); and without addition of nucleic acids (lanes 1, 4, 7).

3.4. Native agarose and zone-interference gel electrophoresis

In native agarose gel electrophoresis, MHV-A59 Nsp10 + Zn, Nsp10 + Fe, and Nsp10 + Co migrated to the cathode at pH 6 due to their positive charge (Fig. 5; the calculated p*I* is 7.2). After incubating Nsp10 with tRNA, double-stranded DNA, or single-stranded RNA, the protein was detected at the anodic side of the application slots (Fig. 5A, lanes 5–7, Fig. 5C, lanes 2, 3, 5, 6, 8, and 9). Thus, the nucleic acids apparently bound to the protein, resulting in negatively charged complexes migrating to the anode. Remarkably, Nsp10 + Co displayed reduced nucleic-acid binding properties compared to proteins produced in the presence of the other two metal ions. ZIGE displayed a pronounced shift of Nsp10 migration in the presence of increasing tRNA concentrations (Fig. 6A). The protein pattern clearly showed that Nsp10 + Zn binding to the negatively charged tRNA increased the electrophoretic mobility towards the anode. The K_d value for the Nsp10 + Zn/tRNA complex was determined as 2.1 ± 0.2 μM (Fig. 6B).

4. Discussion

We have shown in this study that Nsp10 of mouse hepatitis virus binds nucleic acids and metal ions, with a clear preference for zinc over iron and cobalt. The observed stoichiometry is ~2 Zn^{2+} per Nsp10 monomer. Even when cobalt or iron are added in excess to the expression medium, most of the bound metal is zinc, suggesting that zinc ions bind to Nsp10 under physiological conditions of expression in infected cells. A sequence alignment of coronaviral Nsp10 proteins shows that nine of the ten cysteine residues of MHV Nsp10 are strictly

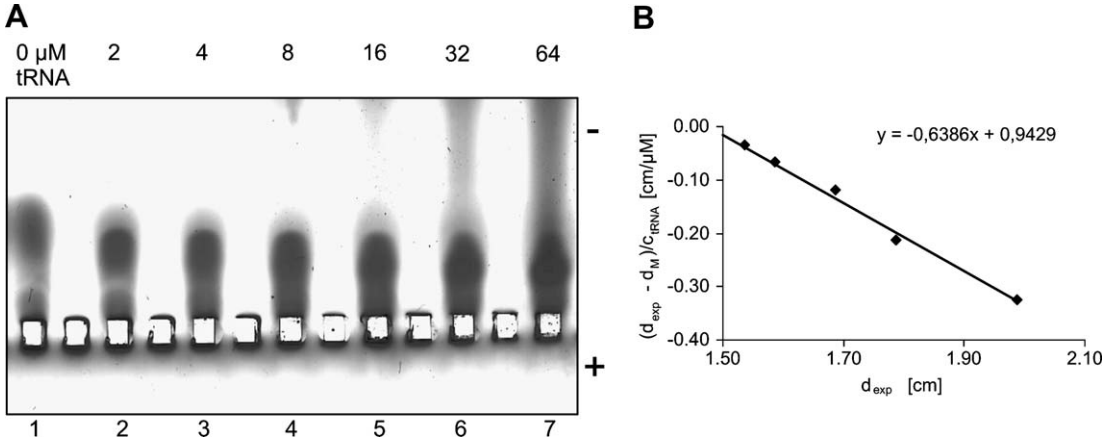

Fig. 6. Complex formation of Nsp10 with tRNA in ZIGE. (A) 40 μM Nsp10 + Zn was present in all sample slots. In lane 1, Nsp10 was not incubated with tRNA. In lanes 2–7, Nsp10 was incubated with increasing amounts of tRNA. (B) Graphical determination of the K_d value for tRNA binding to Nsp10 from the experimental data shown in A, according to the equation given in Section 2. The K_d value is derived from the slope of the graph.

conserved in all three coronavirus groups (Fig. 7). Within its C-terminal half, the motif C74–X_2–C77–X_5–H83–X_6–C90 is found, which could constitute a classical zinc finger of the CCHC type. Residue His83 of this motif is also absolutely conserved throughout the coronaviruses. This motif is followed by a second potential zinc finger displaying the sequence C116–X_2–C119–X_7–C127–X–C129, which would belong to the CCCC type. The presence of more than one zinc finger is quite common in transcription factors. However, we cannot exclude that the conserved Cys residues 17 and 41 of the N-terminal part of Nsp10 may also be involved in complexation of Zn^{2+}, even though they do not match with one of the canonical zinc binding motifs. Cys45 is the only cysteine residue in MHV Nsp10 that is not conserved throughout the *Coronaviridae*, and is therefore unlikely to be involved in metal ion binding.

The presumable Zn-fingers of Nsp10 may function in binding double-stranded RNA. Interestingly, this would make Nsp10 the fourth member of an array of small RNA-binding proteins encoded by the 3′-part of coronavirus replicase orf 1a. Recent structural and biochemical studies showed that also Nsp9 [22,23] (R. Ponnusamy, JRM, RM, and RH, unpublished) and a hexadecameric complex formed by Nsp7 and Nsp8 [24] have RNA-binding properties. These proteins were postulated to be accessory factors for the RdRp complex, a

```
                                      1         11         21         31
1.  MHV A59              100.0%  AGTATEYASN SAILSLCAFS VDPKKTYLDY IKQGGVPVTN
2.  HCoV HKU1             91.1%  AGVATEYAAN SSILSLCAFS VDPKKTYLDY IQQGGVPIIN
3.  HCoV OC43             87.6%  AGTATEYASN SSILSLCAFS VDPKKTYLDF IQQGGTPIAN
4.  TGEV                  57.8%  AGKPTEHPSN SSLLTLCAFS PDPAKAYVDA VKRGMQPVNN
5.  SARS CoV              56.2%  AGNATEVPAN STVLSFCAFA VDPAKAYKDY LASGGQPITN
6.  HCoV NL63             55.6%  AGKQTELAVN SGLLTACAFS VDPATTYLEA VKHGAKPVSN
7.  HCoV 229E             53.3%  AGKQTEFVSN SHLLTHCSFA VDPAAAYLDA VKQGAKPVGN
8.  IBV                   51.5%  -GHETEEVDA VGILSLCSFS VDPADTYCKY VAAGNQPLGN
                                 ~+--++---~ ~-~~~~+~+~ ~++~-~+-~  ~~-+--+~-+

    41         51         61         71         81         91
1.  CVKMLCDHAG TGMAITIKPE ATTNQDSYGG ASVCIYCRSR VEHPDVDGLC KLRGKFVQVP
2.  CVKMLCDHAG TGMAITIKPE ATINQDSYGG ASVCIYCRAR VEHPDVDGIC KLRGKFVQVP
3.  CVKMLCDHAG TGMAITVKPD ATTSQDSYGG ASVCIYCRAR VEHPDVDGLC KLRGKFVQVP
4.  CVKMLSNGAG NGMAVTNGVE ANTQQDSYGG ASVCIYCRCH VEHPAIDGLC RYKGKFVQIP
5.  CVKMLCTHTG TGQAITVTPE ANMDQESFGG ASCCLYCRCH IDHPNPKGFC DLKGKYVQIP
6.  CIKMLSNGAG NGQAITTSVD ANTNQDSYGG ASICLYCRAH VPHPSMDGYC KFKGKCVQVP
7.  CVKMLTNGSG SGQAITCTID SNTTQDTYGG ASVCIYCRAH VAHPTMDGFC QYKGKWVQVP
8.  CVKMLTVHNG SGFAITSKPS PTPDQDSYGG ASVCLYCRAH IAHPNLDGRC QFKGSFVQIP
    +~+++~-~~+ ~+~+~+~---~ ~~~~+~~~++ ++~+~+++-~ ~~++--~+-+ ~~~+~~++~+

    101        111        121        131   137
1.  LGIKDPVSYV LTHDVCQVCG FWRDGSCSCV GTGSQFQ
2.  LGIKDPILYV LTHDVCQVCG FWRDGSCSCV -SSVAVQ
3.  VGIKDPVSYV LTHDVCRVCG FWRDGSCSCV STDTTVQ
4.  TGTQDPIRFC IENEVCVVCG CWLNNGCMCD RTSMQ--
5.  TTCNDPVGFT LRNTVCTVCG MWKGYGCSCD QLREPLMQ
6.  IGCLDPIRFC LENNVCNVCG CWLGHGCACD RTTIQ--
7.  IGTNDPIRFC LENTVCKVCG CWLNHGCTCD RTAIQ--
8.  TTEKDPVGFC LRNKVCTVCQ CWIGHGCQCD SLRQPKSSVQ
    ~~--++---- ~~~~++~++~ -+---~+~+- -~~--~--
```

Fig. 7. Sequence alignment of Nsp10 proteins of coronavirus groups 1, 2, and 3. Sequences were derived from genome sequences of: (1) murine hepatitis virus strain A59 (group 2a; GenBank Accession No. AY597011), (2) human coronavirus HKU1 (group 2a, AY597011), (3) human coronavirus strain OC43 (group 2a, AY39177), (4) transmissible gastroenteritis virus (group 1, AJ271965), (5) SARS coronavirus (group 2b, AY274119), (6) human coronavirus strain NL63 (group 1, AY567487), (7) human coronavirus strain 229E (group 1, AF304460), and (8) infectious bronchitis virus (group 3, M95169). The percentage of sequence identity in comparison to MHV-A59 Nsp10 is indicated. Absolutely conserved residues are marked with a (+), conserved residues are marked with (~), and non-conserved residues are marked with (−). The boxes highlight absolutely conserved cysteine residues.

role that would also be in line with the phenotype of the MHV Nsp10 temperature-sensitive mutant (Gln65 → Glu) recently characterized by Sawicki and colleagues [7].

We have shown here that MHV Nsp10 indeed binds to tRNA and double-stranded oligodeoxynucleotides, and that the K_d for tRNA is ~2 μM. We also showed that binding of Nsp10 to double-stranded DNA leads to dissociation of Nsp10 oligomers, as evident from dynamic light scattering. Zinc fingers are known to be occasionally involved in protein–protein interactions. Therefore, nucleic-acid binding to the presumable zinc fingers of Nsp10 could compete with oligomerization of the protein through these structural features, although we cannot exclude that this could also be due to other interactions. This investigation into the biochemical properties of MHV Nsp10 will add to the functional and structural studies that are currently underway.

Acknowledgements: This work was funded by the VIZIER project of the European Commission (contract No. LSHG-CT-2004-511960; www.vizier-europe.org) and, in part, by the Sino-European Project on SARS Diagnostics and Antivirals (SEPSDA, SP22-CT-2004-003831; www.sepsda.info). R.H. thanks the Fonds der Chemischen Industrie for support. E.S. is grateful to Volker Thiel and Stuart Siddell for providing recombinant vaccinia virus vMHV-inf-1, and acknowledges the general and/or technical support of Clara Posthuma, Linda van der Zanden and Alexander Gorbalenya.

References

[1] Gorbalenya, A.E., Snijder, E.J. and Spaan, W.J.M. (2004) Severe acute respiratory syndrome coronavirus phylogeny: towards consensus. J. Virol. 78, 7863–7866.
[2] Groneberg, D.A., Hilgenfeld, R. and Zabel, P. (2005) Molecular mechanisms of severe acute respiratory syndrome (SARS). Respir. Res. 6, 8–23.
[3] Haring, J. and Perlman, S. (2001) Mouse hepatitis virus. Curr. Opin. Microbiol. 4, 462–466.
[4] Bergmann, C.C., Lane, T.E. and Stohlman, S.A. (2006) Coronavirus infection of the central nervous system. Nat. Rev. Microbiol. 4, 121–132.
[5] Talbot, P.J., Arnold, D. and Antel, J.P. (2001) Virus-induced autoimmune reactions in the CNS. Curr. Top. Microbiol. Immunol. 253, 247–271.
[6] Ziebuhr, J. (2005) The coronavirus replicase. Curr. Top. Microbiol. Immunol. 287, 57–94.
[7] Sawicki, S.G., Sawicki, D.L., Younker, D., Meyer, Y., Thiel, V., Stokes, H. and Siddell, S.G. (2005) Functional and genetic analysis of coronavirus replicase–transcriptase proteins. PLoS Pathogens 1, 1–13.
[8] Ziebuhr, J., Snijder, E.J. and Gorbalenya, A.E. (2000) Virus-encoded proteinases and and proteolytic processing in the Nidovirales. J. Gen. Virol. 81, 853–879.
[9] Ziebuhr, J., Thiel, V. and Gorbalenya, A.E. (2001) The autolytic release of a putative RNA virus transcription factor from its polyprotein precursor involves two paralogous papain-like proteases that cleave the same peptide bond. J. Biol. Chem. 276, 33220–33232.
[10] Anand, K., Palm, G.J., Mesters, J.R., Siddell, S.G., Ziebuhr, J. and Hilgenfeld, R. (2002) Structure of coronavirus main proteinase reveals combination of a chymotrypsin fold with an extra α-helical domain. EMBO J. 21, 3213–3224.
[11] Anand, K., Ziebuhr, J., Wadhwani, P., Mesters, J.R. and Hilgenfeld, R. (2003) Coronavirus main proteinase ($3CL^{pro}$) structure: basis for design of anti-SARS drugs. Science 300, 1763–1767.
[12] Van der Meer, Y., Snijder, E.J., Dobbe, J.C., Schleich, S., Denison, M.R., Spaan, W.J.M. and Krijnse Locker, J. (1999) Localization of mouse hepatitis virus nonstructural proteins and RNA synthesis indicates a role for late endosomes in viral replication. J. Virol. 73, 7641–7657.
[13] Gosert, R., Kanjanahaluethai, A., Egger, D., Bienz, K. and Baker, S.C. (2002) RNA replication of mouse hepatitis virus takes place at double-membrane vesicles. J. Virol. 76, 3697–3708.
[14] Bost, A.G., Prentice, E. and Denison, M.R. (2001) Mouse hepatitis virus replicase protein complexes are translocated to sites of M protein accumulation in the ERGIC at late times of infection. Virology 285, 21–29.
[15] Bost, A.G., Carnahan, R.H., Lu, X.T. and Denison, M.R. (2000) Four proteins processed from the replicase gene polyprotein of mouse hepatitis virus colocalize in the cell periphery and adjacent sites of virion assembly. J. Virol. 74, 3379–3387.
[16] Brockway, S.M., Lu, X.T., Peters, T.A., Dermody, T.S. and Denison, M.R. (2004) Intracellular localization and protein interactions of the gene 1 protein p28 during mouse hepatitis virus replication. J. Virol. 78, 11551–11562.
[17] Ng, L.F.P. and Liu, D.X. (2002) Membrane association and dimerization of a cysteine-rich, 16-kilodalton polypeptide released from the C-terminal region of the coronavirus infectious bronchitis virus 1a polyprotein. J. Virol. 76, 6257–6267.
[18] Gorbalenya, A.E., Koonin, E.V., Donchenko, A.P. and Blinov, V.M. (1989) Coronavirus genome: prediction of putative functional domains in the non-structural polyprotein by comparative amino acid sequence analysis. Nucleic Acids Res. 17, 4847–4861.
[19] Coley, S.E., Lavi, E., Sawicki, S.G., Fu, L., Schelle, B., Karl, N., Siddell, S.G. and Thiel, V. (2005) Recombinant mouse hepatitis virus strain A59 from cloned, full-length cDNA replicates to high titers in vitro and is fully pathogenic in vivo. J. Virol. 79, 3097–3106.
[20] Lowry, O.H., Rosebrough, N.J., Farr, A.L. and Randall, R.J. (1951) Protein measurement with the folin phenol reagent. J. Biol. Chem. 193, 265–275.
[21] Abrahams, J.P., Kraal, B. and Bosch, L. (1988) Zone-interference gel electrophoresis: a new method for studying weak protein–nucleic acid complexes under native equilibrium conditions. Nucleic Acids Res. 16, 10099–10108.
[22] Egloff, M.P., Ferron, F., Campanacci, V., Longhi, S., Rancurel, C., Dutartre, H., Snijder, E.J., Gorbalenya, A.E., Cambillau, C. and Canard, B. (2004) The severe acute respiratory syndrome coronavirus replicative protein nsp9 is a single-stranded RNA-binding subunit unique in the RNA virus world. Proc. Natl. Acad. Sci. USA 16, 3792–3796.
[23] Sutton, G., Fry, E., Carter, L., Sainsbury, S., Walter, T., Nettleship, J., Berrow, N., Owens, R., Gilbert, R., Davidson, A., Siddell, S.G., Poon, L.L., Diprose, J., Alderton, D., Walsh, M., Grimes, J.M. and Stuart, D.I. (2004) The Nsp9 replicase protein of SARS-coronavirus, structure and functional insights. Structure 12, 341–353.
[24] Zhai, Y., Sun, F., Li, X., Pang, H., Xu, X., Bartlam, M. and Rao, Z. (2005) Insights into SARS-CoV transcription and replication from the structure of the nsp7–nsp8 hexadecamer. Nat. Struct. Mol. Biol. 12, 980–986.